RSC Advances

PAPER

View Article Online
View Journal | View Issue

Cite this: *RSC Adv.*, 2021, **11**, 31807

Barium promoted Ni/Sm_2O_3 catalysts for enhanced CO_2 methanation

Nur Athirah Ayub, Hasliza Bahruji * and Abdul Hanif Mahadi

Low temperature CO_2 methanation is a favorable pathway to achieve high selectivity to methane while increasing the stability of the catalysts. A Ba promoted Ni/Sm_2O_3 catalyst was investigated for CO_2 methanation at atmospheric pressure with the temperature ranging from 200–450 °C. 5Ni–5Ba/Sm_2O_3 showed significant enhancement of CO_2 conversion particularly at temperatures ≤ 300 °C compared to Ni/Sm_2O_3. Incorporation of Ba into 5Ni/Sm_2O_3 improved the basicity of the catalysts and transformed the morphology of Sm_2O_3 from random structure into uniform groundnut shape nanoparticles. The uniformity of Sm_2O_3 created interparticle porosity that may be responsible for efficient heat transfer during a long catalytic reaction. Ba is also postulated to catalyze oxygen vacancy formation on Sm_2O_3 under a reducing environment presumably *via* isomorphic substitution. The disappearance of a high temperature (~600 °C) reduction peak in H_2-TPR analysis revealed the reducibility of NiO following impregnation with Ba. However, further increasing the Ba loading to 15% formed $BaNiO_3$–$BaNiO_{2.36}$ phases which consequently reduced the activity of the Ni–Ba/Sm_2O_3 catalyst at low temperature. Ni was suggested to segregate from $BaNiO_3$–$BaNiO_{2.36}$ at high temperature thus exhibiting comparable activity with Ni/Sm_2O_3 at 450 °C.

Received 27th May 2021
Accepted 14th September 2021

DOI: 10.1039/d1ra04115k

rsc.li/rsc-advances

Introduction

Carbon dioxide is a naturally occurring gas occupying ~0.04% of air in the atmosphere. CO_2 is produced from natural processes such as biomass decomposition, or human activities that are associated with the burning of fossil fuel. Primary consumption of fossil fuel as an energy provider results in the rising level of CO_2 in the atmosphere. This greenhouse gas contributes to global warming, which ultimately caused a devastating impact to the environment in particular through extreme climate change.[1] Current analysis by the UNEP (United Nations Environment Programme) indicated that the global temperature was expected to elevate by more than 2 °C by 2050, and more than 4 °C by 2100.[2] Over the years, scientists have investigated multiple approaches to overcome the issue of CO_2 emission. Carbon capture and utilization (CCU) has gain worldwide attention as a method to control CO_2 emission *via* conversion of CO_2 into useful products such as urea and fuel.[3]

Since CO_2 is continuously emitted from industrial processes, the conversion of CO_2 to methane (CH_4) was identified as an ideal route to recycle the most oxidative carbon compound into active carbon species.[4] Catalytic hydrogenation of CO_2 with hydrogen gas produced CH_4 and water, which was discovered by Paul Sabatier in 1902[2] and referred to as the Sabatier reaction or CO_2 methanation (eqn. (1)).

$$CO_2 + 4H_2 \rightleftharpoons CH_4 + 2H_2O,\ \Delta H_{298\ K} = -165\ kJ\ mol^{-1} \quad (1)$$

Since CO_2 methanation is an exothermic reaction, production of methane favors a lower reaction temperature. However as a stable molecule, catalyst was required for the reaction to achieve optimum rate. Competing reactions such as carbon formation (eqn (2)) and reverse-water-gas-shift (RWGS) (eqn (3))[5] occurred predominantly at high temperatures. High temperature reaction also caused coke deposition that eventually contributed to the deactivation of catalysts.

$$CO_2 + 2H_2 \rightleftharpoons C + 2H_2O,\ \Delta H_{298\ K} = -90.1\ kJ\ mol^{-1} \quad (2)$$

$$CO_2 + H_2 \rightleftharpoons CO + H_2O,\ \Delta H_{298\ K} = 41.2\ kJ\ mol^{-1} \quad (3)$$

Metal oxides such as Al_2O_3, TiO_2, ZrO_2 and CeO_2 were commonly investigated as metal supports for Ni-based catalysts.[6] Rare earth element was generally used as promoter to enhance CO_2 methanation primarily due to the high cost of obtaining the element. Sm_2O_3 was often investigated as promoter for various catalytic reaction such as water gas shift reaction,[7] ammonia synthesis,[8] and photocatalytic removal of organic pollutants.[9] As promoter in Co/CeO_2 catalysts, samarium improved the reducibility of Ce^{4+} by facilitating the electron transfer from Co to CeO_2 and enhanced the surface oxygen vacancies.[7] Sm_2O_3 was reported to enhance Ni dispersion, reduced coke deposition, hence enhanced both stability and activity of Ni/SBA-15 catalyst.[10] Ni exhibited high selectivity towards CH_4 and inexpensive, in comparison to noble metals.[5]

Centre of Advanced Material and Energy Sciences, Universiti Brunei Darussalam Jalan Tungku Link, BE 1410, Brunei Darussalam. E-mail: hasliza.bahruji@ubd.edu.bn

The use of alkali and rare earth oxides as promoter further increased the metal-support interaction and metal dispersion.[5] However, Ni was easily sintered during rapid temperature increase and exothermic nature of the methanation reaction. Coke deposition onto the active sites of Ni-based catalysts also caused premature deactivation.[11] W. J. Lee *et al.*[12] stated that highly dispersed Ni particles can be achieved by essentially enhancing the surface defects of the support.

This research aimed to investigate the ability of rare earth metal oxide, Sm_2O_3, as active catalyst for CO_2 methanation reaction. The potential of Sm_2O_3 as support for CO_2 methanation was relied on its basic properties and redox potential, which was ideal to enhance CO_2 adsorption and dissociation. However, studies on Sm_2O_3 as catalysts support for CO_2 methanation was rarely reported. Muroyama *et al.* showed utilization of Ni/Sm_2O_3 as catalyst produced a higher CH_4 yield when compared to Al_2O_3, ZrO_2, CeO_2 and La_2O_3, although the catalysts showed deactivation within 5 h of the reaction.[13] The formation of Sm_2O_3 xerogel *via* epoxide addition method showed high activity and thermal stability of Ni/Sm_2O_3, however 39 wt% of Ni was required to ensure such performances.[14] In this work, $Ni–Ba/Sm_2O_3$ was investigated as catalysts for CO_2 methanation reaction to enhance the activity and the stability of the catalysts. Ba as alkali earth metal was introduced as promoter to enhance the basicity of the catalysts and to improve CO_2 adsorption and dissociation.[15] Ba showed a high affinity towards CO_2 to form carbonate, which was a highly important step towards CO_2 decomposition at mild temperatures.[16] To our knowledge, studies on the effect of Ba as promoter to enhance Ni/Sm_2O_3 activity has not yet been reported. $Ni–Ba/Sm_2O_3$ catalysts was synthesized using wet impregnation method at variation of Ba loading while using 5 wt% of Ni. The enhanced activity was correlated with the basicity, reducibility and morphology of the catalysts determined using FE-SEM, HRTEM, XRD, H_2-TPR, CO_2-TPD and XPS analysis.

Results

XRD analysis

Fig. 1a showed the XRD analysis of Sm_2O_3, $5Ni/Sm_2O_3$ and $5Ni–x Ba/Sm_2O_3$ at different Ba loading (x = 5%, 10% and 15%) after calcination in air at 500 °C. The main characteristic peaks of Sm_2O_3 were observed at $2\theta = 28.2°$, 32.7°, 46.9° and 55.6° which were indexed to (222), (400), (440) and (622) accordingly (JCPDS 043-1029). Following impregnation with Ni and Ba, some of the Sm_2O_3 diffraction peaks were disappeared. As seen in Fig. 1b, narrow angle XRD analysis showed NiO peaks on $5Ni/Sm_2O_3$ and 5Ni-xBa/Sm_2O_3 at $2\theta = 38.9°$ and 42.0°, indexed at (111) and (200) respectively (JCPDS 004-0835), proving that NiO nanoparticles were formed following calcination at 500 °C. However, at 10% of Ba loading, $BaNiO_3$ peak was observed at $2\theta = 18.8°$, 36.8° and 42.3° (JCPDS 072-0403).[17] Increasing the Ba loading to 15%, $BaNiO_{2.36}$ peaks appeared at $2\theta = 21.9°$, 38.3°, 48.9° and 50.4° corresponded to (110), (020), (220), (131), (310) and (240) planes respectively (JCPDS 072-0403). $BaNiO_3$ was reported as less stable than $BaNiO_{2.36}$, which will be decomposed gradually at higher temperatures.[18]

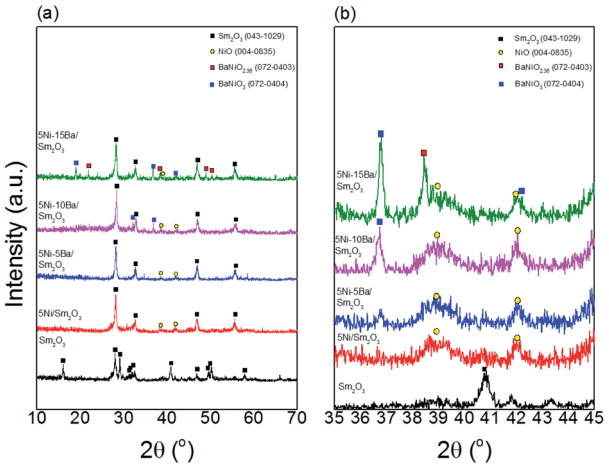

Fig. 1 (a) Wide and (b) narrow angle XRD patterns of pure Sm_2O_3, 5Ni/Sm_2O_3 and 5Ni–*x*Ba on Sm_2O_3 with different Ba loading after calcination at 500 °C.

N_2 adsorption–desorption analysis

The textural properties of $5Ni/Sm_2O_3$ and $5Ni–xBa/Sm_2O_3$ were analyzed using N_2 adsorption–desorption (Fig. 2a). The isotherms of the catalysts were categorized as Type III isotherm with H3-hysteresis loop, according to IUPAC isotherm classification. The H3 loop was related to the adsorbed multi-layer metastability and delayed capillary condensation which occurs in slit-shaped macropores resulted from a low level of pore curvature and flexibility of the aggregate structure.[19,20] The increase of Ba loading slightly enhanced the surface area of the catalysts. $5Ni/Sm_2O_3$ showed 9 m^2/g, and the surface area was enhanced 14 $m^2\ g^{-1}$ for $5Ni–10Ba/Sm_2O_3$. However, the surface area was reduced to 12 $m^2\ g^{-1}$ on $5Ni–15Ba/Sm_2O_3$ presumably due to the formation of $BaNiO_2$. Hysteresis loop presence at high relative pressure (p/p_o > 0.7) implied a broad pore size distribution, comprising both meso- and macropores in the catalysts structure.[21] Pore size distribution analysis (Fig. 2b)

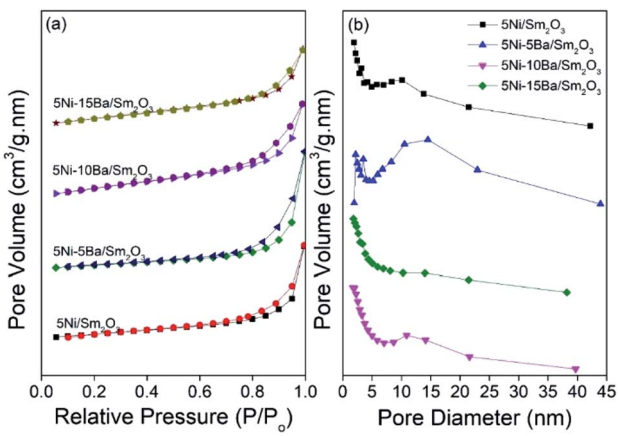

Fig. 2 (a) Nitrogen adsorption–desorption isotherms and (b) pore size distribution of $5Ni/Sm_2O_3$ and $5Ni–xBa/Sm_2O_3$, x = 5%, 10% and 15% after calcination at 500 °C.

Table 1 Textural properties of 5Ni/Sm_2O_3 and 5Ni–x Ba/Sm_2O_3, x = 5%, 10% and 15% Ba loading

Catalyst	S_{BET} (m^2 g^{-1})	Pore volume (cm^3 g^{-1})	Pore size (nm)	T_{H_2} desorption (°C)	H_2 uptake[a] (mmol g_{cat}^{-1})	CO_2 uptake[b] (μmol g_{cat}^{-1})
Sm_2O_3	13	N.D	N.D	410	0.74	6.9
5Ba/Sm_2O_3	N.D	N.D	N.D	526, 555, 863	15.8	13.2
5Ni/Sm_2O_3	9	0.0419	2, 11	412, 516, 635	34.5	10.0
5Ni–5Ba/Sm_2O_3	9	0.0532	3, 15	373, 443, 552	40.9	18.3
5Ni–10Ba/Sm_2O_3	14	0.0414	—	386, 538	97.9	16.5
5Ni–15Ba/Sm_2O_3	12	0.0342	—	495	59.8	6.9

[a] H_2 consumption obtained from H_2-TPR profiles. [b] The amount of adsorbed CO_2 was determined from CO_2-TPD. N.D – not determined.

showed the formation of mesopores on 5Ni–5Ba/Sm_2O_3 catalyst. A broad pore distribution was observed on 5Ni–5Ba/Sm_2O_3 with a slight enhanced of pore volume compared to 5Ni/Sm_2O_3. The data summarized in Table 1 indicated the pore volume was increased to 0.050 cm^3 g^{-1} in 5% Ba loading compared to 0.040 cm^3 g^{-1} in 5Ni/Sm_2O_3 catalyst.

Morphology analysis

Surface morphology of 5Ni/Sm_2O_3 and 5Ni–x Ba/Sm_2O_3 catalysts were characterized using FESEM-EDX and HRTEM analysis. Fig. 3a displayed the morphology of 5Ni/Sm_2O_3 after calcination in air at 500 °C for 3 hours. The SEM image showed a non-uniform crystallites structure with no apparent pattern on the morphology. Following addition of 5% Ba on Ni/Sm_2O_3, the morphology was significantly changed into interconnected uniform nanoparticles resembled to a groundnut-like structure. The presence of uniform pores was observed from the interaction between particles in 5Ni–5Ba/Sm_2O_3 catalyst (Fig. 3b). The addition of Ba significantly reduced the size of crystallites to be within nanoscale length. However, following impregnation with 15% of Ba loading, the uniform groundnut-like structures disappeared and turned into non-uniform crystallites. The uniform porosity was no longer visible as the amount of Ba increased to 15% loading (Fig. 3c). The formation of non-uniform morphology of 5Ni–15Ba/Sm_2O_3 may be associated with the formation of $BaNiO_3$–$BaNiO_{2.36}$ phases as shown in XRD analysis. EDX analysis was carried out to study the Ni and Ba dispersion on Sm_2O_3. EDX mapping (Fig. 3d) of 5Ni–5Ba/Sm_2O_3 showed Ni and Ba particles were evenly dispersed on Sm_2O_3 surface. The homogeneous dispersion can promote synergetic effect between Ni and Ba to improve CO_2 adsorption and to increase catalytic activity.

HRTEM analysis of 5Ni–5Ba/Sm_2O_3 in Fig. 4a and b showed homogeneous dispersion of NiO nanoparticles. The average NiO particle diameter was determined at approximately 3.5 ± 0.5 nm. The interplanar spacing of NiO nanoparticles was measured at 0.21 nm corresponded to (111) plane (16). The interplanar spacing determined at 0.31 nm was in a good agreement with the Sm_2O_3 (222) (d_{222} = 3.142 Å) plane.[22] HRTEM analysis of 5Ni–15Ba/Sm_2O_3 (Fig. 4c and d) estimated the diameter of NiO nanoparticles as 4.5 ± 0.4 nm with interplanar spacing at 0.21 nm. The presence of $BaNiO_{2.36}$ was evident from 0.28 nm crystal plane adjacent to Sm_2O_3.[23]

H_2-TPR analysis

H_2-TPR analysis of the catalysts provided information on the reducibility of NiO and the metal support interaction (Fig. 5). In

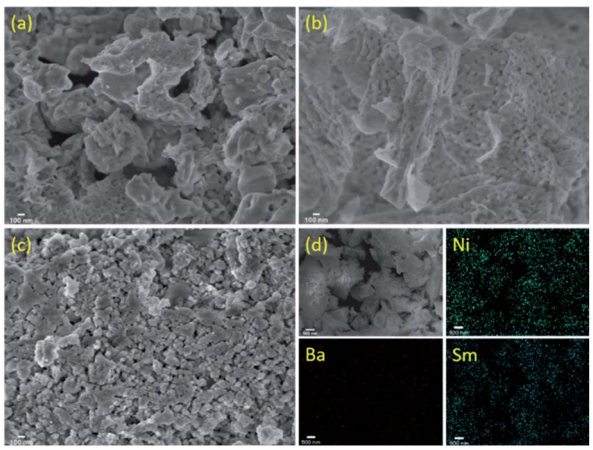

Fig. 3 FESEM images of 5Ni–x Ba/Sm_2O_3 at (a) 0% Ba, (b) 5% Ba, (c) 15% Ba and (d) EDX mapping of 5Ni–x Ba/Sm_2O_3 at 5% Ba after calcination.

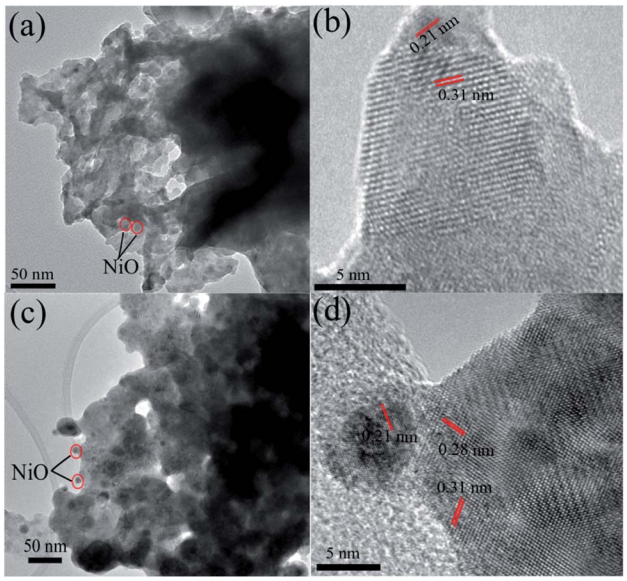

Fig. 4 HRTEM analysis of 5Ni–5Ba/Sm_2O_3 (a and b) and 5Ni–15Ba/Sm_2O_3 (c and d) after calcination in air at 500 °C.

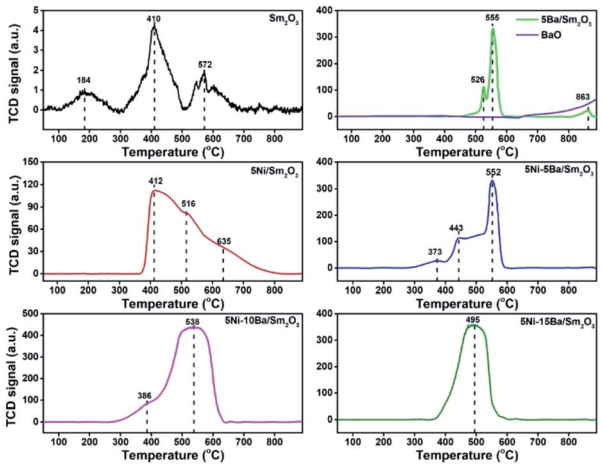

Fig. 5 H_2-TPR profiles of 5Ni/Sm_2O_3, 5Ba/Sm_2O_3, BaO, and 5Ni–*x*Ba/Sm_2O_3 at different Ba loading. The catalysts were calcined in air at 500 °C prior to the analysis.

general, α-type NiO species peak was located at low-temperature region (300–500 °C) signifying bulk NiO particles. β-Type NiO peak can be seen at mild-temperature region (500–700 °C) demonstrating a weak interaction between NiO and support. Meanwhile a high temperature peak >700 °C was assigned to γ-type NiO species with strong interaction with the support.[24–26] Sm_2O_3 only showed a very low H_2 uptake (0.74 mmol g_{cat}^{-1}) suggesting the high stability of Sm_2O_3 which only slightly reduced to SmO. Following impregnation with 5% Ba on Sm_2O_3, sharp TPR peaks appeared at 526 °C and 555 °C, and a small peak at much higher temperatures, 863 °C. The amount of H_2 uptake was increased to 15.2 mmol g_{cat}^{-1}. The H_2 TPR analysis of 5Ba/Sm_2O_3 was compared with H_2 TPR analysis of BaO, which indicated BaO stability under reducing environment. The reduction of Sm_2O_3 upon Ba addition could be due to migration of Ba^{2+} to Sm_2O_3 lattice. The close interaction between Ba^{2+} and Sm^{3+} enhanced the reducibility of Sm^{3+} to Sm^{2+} thus promoting the formation of oxygen vacancy. The hypothesis was postulated from the behaviour of CeO_2 system when doped with cation with a lower charge such as Co^{2+} that leads to charge compensation.[27] This charge compensation mechanism from isomorphic substitution of Ba^{2+} in Sm^{3+} enhanced the formation of surface oxygen vacancies.

All Ni catalysts showed the reduction peaks were formed within α- and β-type ranges and shifted to the lower temperatures with the addition of Ba. 5Ni/Sm_2O_3 showed a broad reduction peaks at 412 °C, with shoulder peaks at 516 °C and 635 °C. The broad reduction peak formation suggested multiple interaction of NiO species with the Sm_2O_3 support.[26] Large NiO particles required a long reduction time and high temperatures in order to ensure complete reduction into its metallic state, hence displayed a broad reduction peak at high temperature region.[21] The H_2-TPR profile of 5Ni–5Ba/Sm_2O_3 showed the appearance of small reduction peak at 373 °C, followed with a broad peak started at 443 °C. A sharp reduction peak at 552 °C showed a similar feature as 5Ba/Sm_2O_3. Impregnation with 5Ni–5Ba on Sm_2O_3 also showed the disappearance of NiO reduction peak at 635 °C which implied the incorporation of Ba into 5Ni/Sm_2O_3 improved the reducibility of NiO nanoparticles. The volume of H_2 consumption was also significantly enhanced with increasing Ba loading presumably due to the combination of H_2 consumption for NiO reduction and the formation of oxygen vacancies on Ba/Sm_2O_3. However, the amount of H_2 uptake was reduced to 59.8 mmol g_{cat}^{-1} on 5Ni–15Ba/Sm_2O_3 presumably due to the formation of $BaNiO_3$–$BaNiO_{2.36}$ phases restricting the evolution of oxygen vacancies.

CO_2-TPD analysis

Surface basicity and distribution of basic sites of 5Ni-*x*Ba/Sm_2O_3 catalysts at different Ba loadings were determined using CO_2-TPD as shown in Fig. 6. CO_2 is a weak Lewis acid that can adsorb on the catalysts to distinguish the types and the strengths of basic sites. The CO_2 desorption peak at temperature below 100 °C was corresponded to CO_2 interaction with a weak basic site on the catalysts surface. This feature was negligible on all catalysts. CO_2-TPD analysis of Sm_2O_3 showed the CO_2 desorption peaks centered at 172 °C and 363 °C that were associated with the medium interaction between CO_2 molecules and moderate basic sites. The peaks formed in the medium basic site region also indicated the formation of carbonate species on the catalysts surface.[28,29] These carbonate species, specifically monodentate carbonate were susceptible towards hydrogenation to form CH_4.[30] Following impregnation of Sm_2O_3 with 5% Ba, the amount of CO_2 uptake was enhanced from 6.9 μmol g_{cat}^{-1} on Sm_2O_3 to 13.2 μmol g_{cat}^{-1} on 5Ba/Sm_2O_3. The CO_2 desorption peak also slightly shifted to lower temperatures. The results clearly showed the presence of Ba enhanced surface basicity of Sm_2O_3. No peak associated with the strong interaction between CO_2 molecules and basic sites was observed at temperature above 500 °C.[21,31] Ni/Sm_2O_3 also showed enhanced CO_2 uptake at 10.9 μmol g_{cat}^{-1}. Synergy between Ni, Ba and Sm_2O_3 was further evidenced on the increase of desorption peak at 150 °C for 5Ni–5Ba/Sm_2O_3 compared to 5Ni/Sm_2O_3 and 5Ba/Sm_2O_3. The amount of adsorbed CO_2 was quantified based on the deconvoluted peak and tabulated in Table 1. The results clearly indicated the addition of Ba into Ni/Sm_2O_3 tremendously

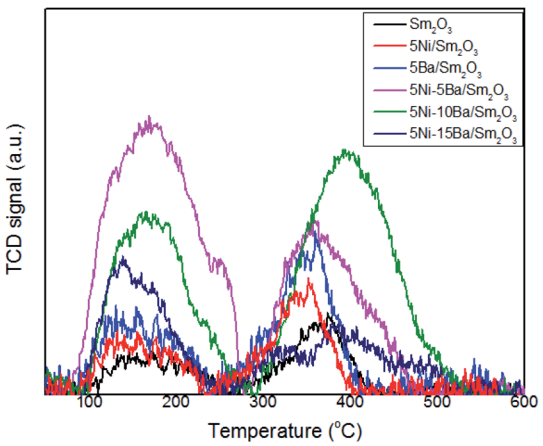

Fig. 6 CO_2-TPD profiles of 5Ni/Sm_2O_3, 5Ba/Sm_2O_3 and 5Ni–*x*Ba/Sm_2O_3 with different Ba loading at x = 5%, 10%, 15%.

improved the surface basicity of the catalysts through the formation of a new basic sites originating from the Ba.[32,33] 5Ni–5Ba/Sm_2O_3 demonstrated the highest CO_2 uptake at 16.5 μmol g_{cat}^{-1}. The role of Ba to provide the additional basic sites was further consolidated by the reduction of CO_2 uptake on 5Ni–15Ba/Sm_2O_3 at 6.9 μmol g_{cat}^{-1}. The formation of $BaNiO_3$–$BaNiO_{2.36}$ as evidenced by the XRD analysis reduced the ability of Ba to increase the surface basicity of the catalyst.

XPS analysis

XPS analysis is a surface analysis method that provided the information of the outer layer of heterogeneous catalysts responsible for catalytic reaction. XPS analysis was conducted following air calcination at 500 °C and reduction at 450 °C (Fig. 7). The presence of Ni and Sm were observed on 5Ni/Sm_2O_3 and 5Ni–5Ba/Sm_2O_3, although Ni 3d signal appeared significantly low in intensity due to the low Ni loading. Analysis of O1s XPS spectra between 5Ni/Sm_2O_3 and 5Ni–5Ba/Sm_2O_3 indicated the presence bulk lattice oxygen. There were no significant differences on the O1s signal following Ba addition. The Sm 3d XPS signal showed doublet peaks appeared at 1083.8 eV and 1150 eV corresponded to Sm^{3+} species.[34] Ni was analyzed at 856.1 eV and 861.8 eV originated from NiO. However, the Ni^0 at 853.1 eV was absent presumably due to the surface oxidation of Ni^0 when the catalyst was exposed to air during the transfer process for XPS measurement.[35] There were no significant differences on the XPS signal of Sm 3d following impregnation with Ba suggesting that no alteration of Sm^{3+} oxidation states. The presence of surface oxygen vacancies on Sm_2O_3 following impregnation with Ba cannot be deduced from the XPS analysis due to the absence of Sm^{2+} peak generally appeared at binding energy ~1095.9 eV and 1121.3 eV.[36,37] XPS also confirmed that dissolution of Ni or Ba into Sm_2O_3 lattice did not take place on the 5Ni–5Ba/Sm_2O_3 catalysts even after reduction at 450 °C.

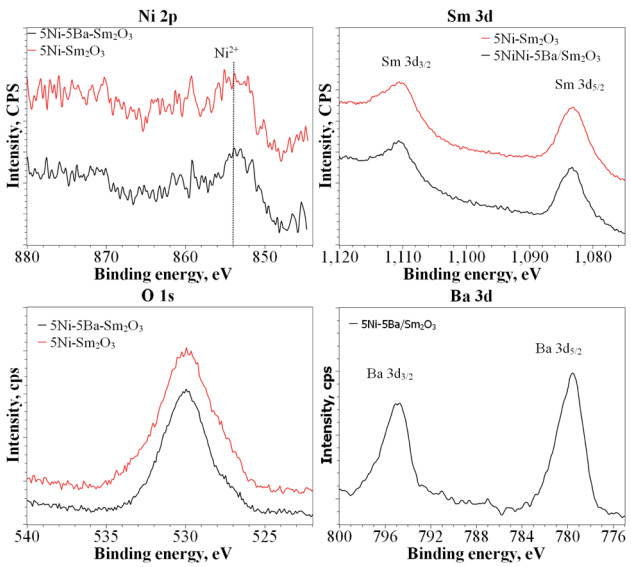

Fig. 7 Ni 2p, Sm 3d, O 1s and Ba 3d XPS spectra of 5Ni/Sm_2O_3 and 5Ni–5Ba/Sm_2O_3 after reduction at 450 °C.

Catalytic activity

The activity of 5Ni/Sm_2O_3 and 5Ni–*x*Ba/Sm_2O_3 on the variation of Ba loading was investigated at 200–450 °C (Fig. 8). No activity was observed at 200 °C, and all the catalysts showed CO_2 conversion at 250 °C with 100% selectivity to methane. Increasing the temperature to 300 °C significantly enhanced the conversion of CO_2. 5Ni–5Ba/Sm_2O_3 showed the highest CO_2 conversion at 38.9% followed with 5Ni–10Ba/Sm_2O_3 at 29%. The conversion was significantly higher than 5Ni/Sm_2O_3 with only 20% at 300 °C. 5Ni–15Ba/Sm_2O_3 was less active than 5Ni/Sm_2O_3 at temperature below 350 °C presumably due to the formation of $BaNiO_2$. Evidently, as the amount of Ba loading increased to 10% and 15%, the CO_2 conversions were comparable with 5Ni/Sm_2O_3 at 400 °C and 450 °C. Reaction at 450 °C showed 72.7% of CO_2 conversion on 5Ni–5Ba/Sm_2O_3, which was slightly higher than 5Ni/Sm_2O_3, 5Ni–10Ba/Sm_2O_3 and 5Ni–15Ba/Sm_2O_3 at ~66.8%. It is apparent that the addition of Ba enhanced the activity of Ni catalysts at temperature below 350 °C. Meanwhile at temperature above 400 °C, the reaction was dictated by the thermodynamic of the reaction thus restricting the catalytic performances of all the catalysts. It is also interesting to note that all the 5Ni/Sm_2O_3 and 5Ni–*x*Ba/Sm_2O_3 catalysts exhibited 100% selectivity to methane. When the Ni–Ba/Sm_2O_3 catalysts were compared with the results previously reported on Ni/metal oxides (Table 2), it is apparent that Ni–Ba/Sm_2O_3 selectively transformed CO_2 to methane and prevented CO formation. The activity of 5Ni–5Ba/Sm_2O_3 was further investigated for 28 h to show the stability of the catalysts (Fig. 9). The conversion was observed at 39% with 100% selectivity towards methane, with similar conversion was observed up to 28 h.

Fig. 10 summarized the effect of reduction temperature on the activity of 5Ni/Sm_2O_3 and 5Ni–5Ba/Sm_2O_3 in order to further elucidate the role of Ba in enhancing Ni activity. These studies also provided insight into the importance of reducing the catalysts prior to the reaction, to ensure the catalysts gained high catalytic activity. Reduction at 250 °C showed the CO_2 conversion of 5Ni/Sm_2O_3 was significantly lower in comparison to 5Ni–5Ba/Sm_2O_3. 5Ni/Sm_2O_3 was only active at 350 °C, to give

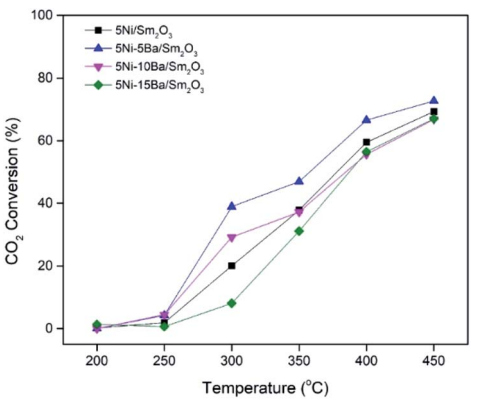

Fig. 8 CO_2 conversion for 5Ni/Sm_2O_3 and 5Ni–*x*Ba/Sm_2O_3 at $x = 5\%$, 10%, 15%. The catalysts was pre-reduced *in situ* under H_2 for 3 h at 450 °C.

Table 2 Catalytic performance comparison among various Ni-based catalysts prepared using wet impregnation as CO_2 methanation catalysts

Catalysts	Reaction condition	X_{CO_2} (%)	S_{CH_4} (%)	Reference
$5Ni/Sm_2O_3$	450 °C, 1 bar	69.3	100	This work
$5Ni–5Ba/Sm_2O_3$	450 °C, 1 bar	72.7	100	This work
$5Ni–10Ba/Sm_2O_3$	450 °C, 1 bar	66.8	100	This work
$5Ni–15Ba/Sm_2O_3$	450 °C, 1 bar	67.0	100	This work
5Ni/NaY-DM	400 °C, 1 bar	67	94	39
5Ni/MSN	300 °C, 1 bar	64.1	99.9	40
$10Ni/SiO_2$	400 °C, 1 bar	73.2	98.7	41
10Ni/MgO	400 °C, 1 bar	28.9	9.0	
$10Ni/SiO_2$ + 10Ni/MgO	400 °C, 1 bar	66.5	96.8	
$10Ni/CeO_2$	350 °C, 1 bar	79.1	76.5	42
$5Ni/CZ_{imp}$	350 °C, 1 bar	59.8	97.3	30

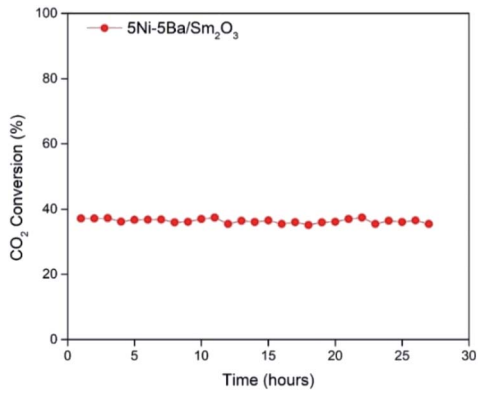

Fig. 9 Catalytic stability of $5Ni–5Ba/Sm_2O_3$ catalysts at 300 °C for 28 h.

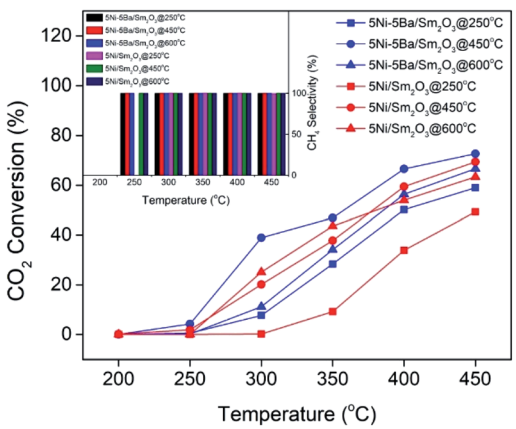

Fig. 10 CO_2 conversion and selectivity of $5Ni/Sm_2O_3$ and $5Ni–5Ba/Sm_2O_3$ at different reduction temperature.

9.2% of CO_2 conversion. The result was indirect contrast to $5Ni–5Ba/Sm_2O_3$, in which 7.9% conversion was analysed at 300 °C following pre-reduction at 250 °C and increased to 28.4% at 350 °C. When the reaction temperature was further increased to 450 °C, the conversion was enhanced to give 49% for $5Ni/Sm_2O_3$ and 59% for $5Ni–5Ba/Sm_2O_3$. Following reduction at 450 °C, no methane was produced at 200 °C but significant conversion was observed at 250 °C for both catalysts. $5Ni–5Ba/Sm_2O_3$ showed 4.3% conversion at 250 °C meanwhile Ni/Sm_2O_3 only showed 1.9% of CO_2 conversion. Increasing the reaction temperature to 300 °C, further increased CO_2 conversion of 39% on Ba promoted catalysts compared to reduction at 250 °C with only 7.7%. When $5Ni/Sm_2O_3$ was reduced at 600 °C, the catalysts achieved 24% of CO_2 conversion at 300 °C, slightly higher than $5Ni/Sm_2O_3$ reduced at 450 °C. Fully reduction of NiO at 600 °C according to H_2-TPR analysis (Fig. 5) was suggested to improve $5Ni/Sm_2O_3$ activity. However, reduction of $5Ni–5Ba/Sm_2O_3$ at 600 °C reduced the CO_2 conversion. H_2-TPR analysis of $5Ni–5Ba/Sm_2O_3$ showed the catalyst was fully reduced at temperature below 500 °C, thus high temperature reduction may cause particle sintering.[38] Nevertheless, all the catalysts showed 100% selectivity towards CH_4. The results obtained on the effect of reduction temperature is highly important to show the role of Ba in improving the activity of Ni catalysts particularly for CO_2 methanation at low temperature.

Discussions

The effect of Ba on Ni/Sm_2O_3 activity was observed particularly when the reaction was carried out at temperature below 300 °C. The activity of most nickel catalysts for CO_2 methanation was reported to have insignificant increment at the temperature above 350 °C mainly due to the thermodynamic restriction.[43] Reaction at temperatures above 400 °C showed the gap between CO_2 conversions on $5Ni–5Ba/Sm_2O_3$ and $5Ni/Sm_2O_3$ were only slightly varied. At low temperature, the methanation was restricted by kinetic due to the stability of CO_2.[44] The results proved the synergy between Ni,Ba and Sm_2O_3 for CO_2 conversion at mild temperatures. The combination of increased basicity, surface oxygen vacancies, NiO reducibility and interparticle meso-porosity of $5Ni–5Ba/Sm_2O_3$ enhanced the activity and stability of $5Ni–xBa/Sm_2O_3$ catalyst. It is also interesting to note that, $5Ni–5Ba/Sm_2O_3$ exhibited 100% selectivity towards methane even when the reaction was carried out at 450 °C. Sm_2O_3 is a rare earth metal oxide, with mild basicity and redox properties which is ideal for CO_2 adsorption and hydrogenation. Barium as alkali earth metal promoter further enhanced the basicity of the catalysts evidenced by the increase of adsorbed CO_2 volume determined using CO_2-TPD. There is

a possibility that introduction of Ba^{2+} in Sm_2O_3 enhanced the mobility of oxygen species consequently facilitated the formation of oxygen vacancies on reducible metal oxides.[45] The presence of surface oxygen vacancies during catalytic reaction promotes CO_2 activation and dissociation.[46] Although the XPS analysis showed no evidence of Sm^{2+} species, there is a possibility that Sm_2O_3 as redox active metal oxide, to be responded with the changes of oxidation states under reducing environment, alternating between Sm^{3+} to Sm^{2+}.[34] CO_2 adsorbed on the metal oxide surface to form monodentate or bidentate carbonate species depending on the oxygen vacancies within the vicinity of Ni nanoparticles.[28] Furthermore, the presence of surface oxygen vacancies on Sm_2O_3 following the addition of Ba enhanced the hydrogenation of carbonate into formate intermediates.[28] Formate intermediate will further undergo C–O dissociation and hydrogen insertion to form methane, thus preventing decomposition into CO.[28]

However at higher Ba loading (15%), the formation of $BaNiO_3$–$BaNiO_{2.36}$ was observed after calcination at 500 °C. $BaNiO_{2.36}$ is a stable crystalline phase resulting from the oxidation of Ba and Ni precursors to form zig-zag chains of Ni^{2+} ion.[47] The average oxidation states of Ni in $BaNiO_2$ is 2+, and it is interchangeable to 4+ under oxygen at high temperature to form $BaNiO_3$.[17] Since it was crucial for Ni to be in its reduction state in order to catalyze hydrogen dissociation in CO_2 methanation reaction,[48] the formation of $BaNiO_3$–$BaNiO_{2.36}$ reduced the activity of 5Ni–15Ba/Sm_2O_3. Furthermore, $BaNiO_3$–$BaNiO_{2.36}$ inhibited the contribution of Ba as the additional basic sites evidenced by the CO_2-TPD analysis thus resulting in a low catalytic activity at temperature below 350 °C. However, as the temperature was increased to 450 °C, there is a possibility that NiO segregating from $BaNiO_3$–$BaNiO_{2.36}$ under the presence of H_2. Although we have no evidence on the segregation of NiO from $BaNiO_2$ during reaction at 450 °C, the comparable activity with Ni/Sm_2O_3 implied such processes may occur *in situ* under the flow of reactant gases.

Impregnation of barium also altered the morphology of Sm_2O_3 to form uniform particles within ~100 nm of size with interparticle porosity. It is suggested that partial dissolution of Sm_2O_3 during impregnation changed the morphology, which was essential to improve the uniformity of nanoparticles. The formation of uniform nanoparticles with interparticle porosity may be beneficial to facilitate carbon dioxide adsorption and diffusion in order to react with the dissociated H atom on Ni sites to form CH_4.[5,49] Porosity was also improved the heat transfer capacity that allowed the catalysts to overcome the heat released during the exothermic reaction.[50]

Experimental

Catalysts preparation

All the catalysts were prepared using wetness impregnation method. Nickel(III) nitrate hexahydrate was obtained from Emsure, 99.0%, barium nitrate from Emsure, 99.0%, samarium oxide from Aldrich, 99%. 5Ni–*x*Ba/Sm_2O_3 catalysts were prepared with different Ba loading, and x = 5 wt%, 10 wt% and 15 wt%. The amount of Ni was kept at 5 wt% relative to the weight of Sm_2O_3. $Ba(NO_3)_2$, $Ni(NO_3)_2$ and Sm_2O_3 were weighed accordingly and physically mixed, which later then dissolved in 10 mL of distilled water. The mixture was stirred continuously for 3 h at 60 °C to ensure thorough dispersion. The catalysts were dried at 200 °C for 2 hours and then calcined at 500 °C for 3 hours in air atmosphere with a heating rate of 10 °C min^{-1}.

Catalyst characterization

Field Emission Scanning Electron Microscope (JSM-7610F equipped with EDX) was used to investigate the surface morphology of the catalysts. Energy Dispersive X-ray analysis was carried out to determine the Ni and Ba dispersion onto Sm_2O_3. The morphological analysis at micro and nano-scales resolution was carried out using high-resolution field emission transmission electron microscopy (HRTEM) Tecnai G2 F20 STWIN at 200 kV. Prior to the analysis, the catalyst was ground and dispersed in water, and the suspension was dropped on the TEM grid and leave to dry at ambient condition. X-ray powder diffraction (Shimadzu XRD-700 X-ray Diffractometer) was carried out to analyze the crystalline structure of the catalysts by utilizing Cu-Kα radiation at λ = 1.54 Å, with operating conditions of 60 kV and 50 mA. The scanning angle range, 2θ, was 10–70° with a scan rate of 2° min^{-1}. The crystalline structure size was calculated using Scherrer's equation (eqn (4)).

$$D = \frac{k\lambda}{\beta \cos \theta} \quad (4)$$

where D is the crystallite size (nm), λ is the wavelength of X-ray (0.15406 nm), θ is the peak position (radians), k is Scherrer constant and β is the FWHM (radians).

Surface area, average pore volume and pore diameter of 5Ni/Sm_2O_3 and 5Ni–*x*Ba/Sm_2O_3 at different Ba loading were determined using N_2 adsorption at 77 K (Micromeritics ASAP 2020). The samples were degassed under carbon degassing conditions for 2 hours at 300 °C. Brunauer–Emmett–Teller (BET) equation was used to calculate the surface area and Barret–Joyner–Halenda (BJH) equation for pore volume and diameter calculation. The pore volume was determined based on three different measurement with standard deviation was measured at 8.91×10^{-5}. X-ray photoelectron spectra (XPS) were recorded on a Kratos Axis Ultra-DLD XPS spectrometer with a monochromatic Al kα source (75–150 W) and analyser pass energies of 160 eV (for survey scans) or 40 eV (for detailed scans). The XPS data was analysed using CASA XPS software and all the samples were calibrated by adjusting the C 1s position to 284.5 eV. H_2 temperature-programmed reduction (Quantachrome ChemBET Pulsar TPR/TPD, equipped with TCD) was performed to study the reducibility of the catalyst. Catalyst was pre-treated in N_2 stream with flow of 75 mL min^{-1} at 100 °C for 1 hour and cooled down to 40 °C. The catalysts were heated to 900 °C with a heating rate of 10°C min^{-1} in a 5% H_2/N_2 gas mixture with a flow rate of 75 mL min^{-1}. CO_2 temperature-programmed desorption was conducted to study the surface basicity and basic sites distribution of the catalysts. Catalysts were heated to 600 °C for 1 hour under 5% H_2/N_2 gases, which later cooled to room temperature under He flow. Catalyst was exposed to CO_2 gas stream for 30 minutes and then flushed out

with He for 1 hour. TPD was finally carried out from 40–600 °C with a heating rate of 10 °C min^{-1}.

Catalytic activity

CO_2 methanation reaction was conducted in a stainless-steel plug flow reactor at atmospheric pressure and reaction temperature ranging from 200 to 450 °C. 0.5 g of catalyst was placed in a tubular fixed bed reactor and reduced *in situ* with H_2 gas (99.9%) with flow rate of 20 mL min^{-1} at 450 °C for 3 h. The catalyst was cooled down to room temperature and $CO_2/H_2/N_2$ (15%/60%/25%) gases at 20 mL min^{-1} were flowed in the reactor. The gas effluent from the reactor was analyzed by GC (Shimadzu GC-2014 with TCD detector). Reaction temperature was increased by 50 °C every hour and the gas were sampled using GC. CO_2 conversion (eqn (5)), CH_4 selectivity (eqn (6)) and CO selectivity (eqn (7)), and CH_4 yield (eqn (8)) were calculated according to the previous method (ref. 48) as follows:

$$x_{CO_2} = \left[\frac{m_{CH_4} + m_{CO}}{m_{CO_2} + m_{CH_4} + m_{CO}}\right] \times 100\% \quad (5)$$

$$S_{CH_4} = \left[\frac{m_{CH_4}}{m_{CH_4} + m_{CO}}\right] \times 100\% \quad (6)$$

$$S_{CO} = \left[\frac{m_{CO}}{m_{CH_4} + m_{CO}}\right] \times 100\% \quad (7)$$

$$Y_{CH_4} = x_{CO_2} S_{CH_4} \quad (8)$$

where x_{CO_2}(%) is the CO_2 conversion, S_{CH_4}(%) is the CH_4 selectivity, S_{CO}(%) is the CO selectivity, Y_{CH_4}(%) is the CH_4 yield and m is the number of moles of the gases.

Conclusions

The activity of Ni–Ba/Sm_2O_3 catalysts was investigated to enhance CO_2 methanation at moderate reaction temperatures. 5Ni–5Ba/Sm_2O_3 demonstrated a higher CO_2 conversion with 100% CH_4 selectivity in comparison to 5Ni/Sm_2O_3. The effect of increasing Ba loading on 5Ni/Sm_2O_3 exhibited the changes of porosity and uniformity of the catalysts structure, and the reducibility of NiO. Ba as promoter also enhanced the number of basic sites and surface oxygen vacancies, and transformed the non-uniform aggregates Sm_2O_3 into uniform size nanoparticles. The basicity originated from Ba promoter enhanced CO_2 adsorption meanwhile the porosity facilitated the heat transfer process during catalytic reaction which consequently increased the catalytic stability. However, further increasing the Ba loading to 15% destroyed the uniform nanostructure and porosity of the catalysts, due to the formation of $BaNiO_3$–$BaNiO_{2.36}$ phases thus reducing the catalytic performance at low temperatures.

Conflicts of interest

There are no conflicts to declare.

Acknowledgements

The authors would like to acknowledge UBD University Research Grant for funding this research (UBD/RSCH/URC/RG(b)/2019/012).

Notes and references

1 T. R. Anderson, E. Hawkins and P. D. Jones, CO_2, the greenhouse effect and global warming: from the pioneering work of Arrhenius and Callendar to today's Earth System Models, *Endeavour*, 2016, **40**(3), 178–187, DOI: 10.1016/j.endeavour.2016.07.002.

2 W. Li, H. Wang, X. Jiang, J. Zhu, Z. Liu, X. Guo, *et al.*, A short review of recent advances in CO_2 hydrogenation to hydrocarbons over heterogeneous catalysts, *RSC Adv.*, 2018, **8**(14), 7651–7669, DOI: 10.1039/C7RA13546G.

3 R. M. Cuéllar-Franca and A. Azapagic, Carbon capture, storage and utilisation technologies: A critical analysis and comparison of their life cycle environmental impacts, *J CO_2 Util.*, 2015, **9**, 82–102.

4 N. M. Martin, P. Velin, M. Skoglundh, M. Bauer and P. A. Carlsson, Catalytic hydrogenation of CO_2 to methane over supported Pd, Rh and Ni catalysts, *Catal. Sci. Technol.*, 2017, **7**(5), 1086–1094, DOI: 10.1039/C6CY02536F.

5 J. Ashok, S. Pati, P. Hongmanorom, Z. Tianxi, C. Junmei and S. Kawi, A review of recent catalyst advances in CO_2 methanation processes, *Catal. Today*, 2020, **356**, 471–489, DOI: 10.1016/j.cattod.2020.07.023.

6 K. Stangeland, D. Kalai, H. Li and Z. Yu, CO_2 Methanation: The Effect of Catalysts and Reaction Conditions, *Energy Procedia*, 2017, **105**(1876), 2022–2027.

7 P. Tepamatr, N. Laosiripojana, T. Sesuk and S. Charojrochkul, Effect of samarium and praseodymium addition on water gas shift performance of Co/CeO_2 catalysts, *J. Rare Earths*, 2020, **38**(11), 1201–1206, DOI: 10.1016/j.jre.2019.12.003.

8 Z. Chunhui, Z. Yifeng and L. Huazhang, Effect of samarium on methanation resistance of activated carbon supported ruthenium catalyst for ammonia synthesis, *J. Rare Earths*, 2010, **28**(4), 552–555, DOI: 10.1016/S1002-0721(09)60152-6.

9 S. Singh, P. Kaur, V. Kumar, K. B. Tikoo and S. Singhal, Traversing the advantageous role of samarium doped spinel nanoferrites for photocatalytic removal of organic pollutants, *J. Rare Earths*, 2020, DOI: 10.1016/j.jre.2020.12.008.

10 Z. Taherian, M. Yousefpour, M. Tajally and B. Khoshandam, A comparative study of ZrO_2, Y_2O_3 and Sm_2O_3 promoted Ni/SBA-15 catalysts for evaluation of CO_2/methane reforming performance, *Int. J. Hydrogen Energy*, 2017, **42**(26), 16408–16420.

11 X. L. Wang, M. Yang, L. J. Zhu, X. N. Zhu and S. R. Wang, CO_2 methanation over Ni/Mg@MCM-41 prepared by in situ synthesis method, *J. Fuel Chem. Technol.*, 2020, **48**(4), 456–465, DOI: 10.1016/S1872-5813(20)30020-7.

12 W. J. Lee, C. Li, H. Prajitno, J. Yoo, J. Patel, Y. Yang, *et al.*, Recent trend in thermal catalytic low temperature CO_2

methanation: A critical review, *Catal. Today*, 2021, **368**, 2–19, DOI: 10.1016/j.cattod.2020.02.017.

13 H. Muroyama, Y. Tsuda, T. Asakoshi, H. Masitah, T. Okanishi, T. Matsui, *et al.*, Carbon dioxide methanation over Ni catalysts supported on various metal oxides, *J. Catal.*, 2016, **343**, 178–184, DOI: 10.1016/j.jcat.2016.07.018.

14 J. Ilsemann, A. Sonström, T. M. Gesing, R. Anwander and M. Bäumer, Highly Active Sm_2O_3–Ni Xerogel Catalysts for CO_2 Methanation, *ChemCatChem*, 2019, **11**(6), 1732–1741.

15 N. A. Sholeha, S. Mohamad, H. Bahruji, D. Prasetyoko, N. Widiastuti, N. A. Abdul Fatah, *et al.*, Enhanced CO_2 methanation at mild temperature on Ni/zeolite from kaolin: Effect of metal-support interface, *RSC Adv.*, 2021, **11**(27), 16376–16387.

16 A. Bansode, B. Tidona, P. R. Von Rohr and A. Urakawa, Impact of K and Ba promoters on CO_2 hydrogenation over Cu/Al_2O_3 catalysts at high pressure, *Catal. Sci. Technol.*, 2013, **3**(3), 767–778.

17 A. M. Arévalo-López, M. Huvé, P. Simon and O. Mentré, The hidden story in $BaNiO_3$ to $BaNiO_2$ transformation: Adaptive structural series and NiO exsolution, *Chem. Commun.*, 2019, **55**(26), 3717–3720.

18 M. Liu, Z. Wang, M. Liu, X. Li, K. Blinn, S. Lai, *et al.*, Understanding the phase formation and compositions of barium carbonate modified NiO-yttria stabilized zirconia for fuel cell applications, *Int. J. Hydrogen Energy*, 2015, **40**(45), 15597–15604, DOI: 10.1016/j.ijhydene.2015.09.092.

19 Z. A. Alothman, A review: Fundamental aspects of silicate mesoporous materials, *Materials*, 2012, **5**(12), 2874–2902.

20 K. S. W. Sing and R. T. Williams, Physisorption hysteresis loops and the characterization of nanoporous materials, *Adsorpt. Sci. Technol.*, 2004, **22**(10), 773–782.

21 C. Italiano, J. Llorca, L. Pino, M. Ferraro, V. Antonucci and A. Vita, CO and CO_2 methanation over Ni catalysts supported on CeO_2, Al_2O_3 and Y_2O_3 oxides, *Appl. Catal., B*, 2020, **264**, 118494.

22 B. T. Sone, E. Manikandan, A. Gurib-Fakim and M. Maaza, Sm_2O_3 nanoparticles green synthesis via Callistemon viminalis' extract, *J. Alloys Compd.*, 2015, **650**, 357–362, DOI: 10.1016/j.jallcom.2015.07.272.

23 M. Retuerto, F. Calle-Vallejo, L. Pascual, P. Ferrer, Á. García, J. Torrero, *et al.*, Role of lattice oxygen content and Ni geometry in the oxygen evolution activity of the Ba–Ni–O system, *J. Power Sources*, 2018, **404**(September), 56–63, DOI: 10.1016/j.jpowsour.2018.09.098.

24 A. Quindimil, U. De-La-Torre, B. Pereda-Ayo, A. Davó-Quiñonero, E. Bailón-García, D. Lozano-Castelló, *et al.*, Effect of metal loading on the CO_2 methanation: A comparison between alumina supported Ni and Ru catalysts, *Catal. Today*, 2020, **356**, 419–432.

25 C. Jiménez-González, Z. Boukha, B. De Rivas, J. J. Delgado, M. Á. Cauqui, J. R. González-Velasco, *et al.*, Structural characterisation of Ni/alumina reforming catalysts activated at high temperatures, *Appl. Catal., A*, 2013, **466**, 9–20, DOI: 10.1016/j.apcata.2013.06.017.

26 C. Lv, L. Xu, M. Chen, Y. Cui, X. Wen, C. e. Wu, *et al.*, Constructing highly dispersed Ni based catalysts supported on fibrous silica nanosphere for low-temperature CO_2 methanation, *Fuel*, 2020, **278**, 118333.

27 K. Polychronopoulou, A. A. Alkhoori, A. M. Efstathiou, M. A. Jaoude, C. M. Damaskinos, M. A. Baker, *et al.*, Design Aspects of Doped CeO_2 for Low-Temperature Catalytic CO Oxidation: Transient Kinetics and DFT Approach, *ACS Appl. Mater. Interfaces*, 2021, **13**(19), 22391–22415.

28 S. Wang, Q. Pan, J. Peng and S. Wang, In situ FTIR spectroscopic study of the CO_2 methanation mechanism on $Ni/Ce_{0.5}Zr_{0.5}O_2$, *Catal. Sci. Technol.*, 2014, **4**(2), 502–509.

29 M. J. Kim, J. R. Youn, H. J. Kim, M. W. Seo, D. Lee, K. S. Go, *et al.*, Effect of surface properties controlled by Ce addition on CO_2 methanation over $Ni/Ce/Al_2O_3$ catalyst, *Int. J. Hydrogen Energy*, 2020, **45**(46), 24595–24603, DOI: 10.1016/j.ijhydene.2020.06.144.

30 P. A. U. Aldana, F. Ocampo, K. Kobl, B. Louis, F. Thibault-Starzyk, M. Daturi, *et al.*, Catalytic CO_2 valorization into CH_4 on Ni-based ceria-zirconia. Reaction mechanism by operando IR spectroscopy, *Catal. Today*, 2013, **215**, 201–207, DOI: 10.1016/j.cattod.2013.02.019.

31 K. Zhao, W. Wang and Z. Li, Highly efficient Ni/ZrO_2 catalysts prepared via combustion method for CO_2 methanation, *J CO_2 Util.*, 2016, **16**, 236–244.

32 A. Quindimil, U. De-La-Torre, B. Pereda-Ayo, J. A. González-Marcos and J. R. González-Velasco, Ni catalysts with La as promoter supported over Y- and BETA- zeolites for CO_2 methanation, *Appl. Catal., B*, 2018, **238**(April), 393–403, DOI: 10.1016/j.apcatb.2018.07.034.

33 D. Wierzbicki, R. Debek, M. Motak, T. Grzybek, M. E. Gálvez and P. Da Costa, Novel Ni-La-hydrotalcite derived catalysts for CO_2 methanation, *Catal. Commun.*, 2016, **83**, 5–8.

34 G. K. Hodgson, S. Impellizzeri, G. L. Hallett-Tapley and J. C. Scaiano, Photochemical synthesis and characterization of novel samarium oxide nanoparticles: Toward a heterogeneous Brønsted acid catalyst, *RSC Adv.*, 2015, **5**(5), 3728–3732.

35 H. Bahruji, M. Bowker, P. R. Davies, J. Kennedy and D. J. Morgan, The importance of metal reducibility for the photoreforming of methanol on transition metal-TiO_2 photocatalysts and the use of non-precious metals, *Int. J. Hydrogen Energy*, 2015, **40**(3), 1465–1471, DOI: 10.1016/j.ijhydene.2014.11.097.

36 T. D. Nguyen, D. Mrabet and T. O. Do, Controlled self-assembly of Sm_2O_3 nanoparticles into nanorods: Simple and large scale synthesis using bulk Sm_2O_3 powders, *J. Phys. Chem. C*, 2008, **112**(39), 15226–15235.

37 T. D. Nguyen, C. T. Dinh and T. O. Do, Monodisperse samarium and cerium orthovanadate nanocrystals and metal oxidation states on the nanocrystal surface, *Langmuir*, 2009, **25**(18), 11142–11148.

38 M. Aghayan, D. I. Potemkin, F. Rubio-Marcos, S. I. Uskov, P. V. Snytnikov and I. Hussainova, Template-Assisted Wet-Combustion Synthesis of Fibrous Nickel-Based Catalyst for Carbon Dioxide Methanation and Methane Steam Reforming, *ACS Appl. Mater. Interfaces*, 2017, **9**(50), 43553–43562.

39 N. A. Sholeha, L. Jannah, H. N. Rohma, N. Widiastuti, D. Prasetyoko, A. A. Jalil, *et al.*, Synthesis of zeolite NaY from dealuminated metakaolin as Ni support CO_2 hydrogenation to methane, *Clays Clay Miner.*, 2020, **68**(5), 513–523.

40 M. A. A. Aziz, A. A. Jalil, S. Triwahyono, R. R. Mukti, Y. H. Taufiq-Yap and M. R. Sazegar, Highly active Ni-promoted mesostructured silica nanoparticles for CO_2 methanation, *Appl. Catal., B*, 2014, **147**, 359–368.

41 M. Guo and G. Lu, The effect of impregnation strategy on structural characters and CO_2 methanation properties over MgO modified Ni/SiO_2 catalysts, *Catal. Commun.*, 2014, **54**, 55–60, DOI: 10.1016/j.catcom.2014.05.022.

42 S. Tada, T. Shimizu, H. Kameyama, T. Haneda and R. Kikuchi, Ni/CeO_2 catalysts with high CO_2 methanation activity and high CH_4 selectivity at low temperatures, *Int. J. Hydrogen Energy*, 2012, **37**(7), 5527–5531, DOI: 10.1016/j.ijhydene.2011.12.122.

43 F. Ocampo, B. Louis, L. Kiwi-Minsker and A. C. Roger, Effect of Ce/Zr composition and noble metal promotion on nickel based $Ce_xZr_{1-x}O_2$ catalysts for carbon dioxide methanation, *Appl. Catal., A*, 2011, **392**(1–2), 36–44, DOI: 10.1016/j.apcata.2010.10.025.

44 I. Champon, A. Bengaouer, A. Chaise, S. Thomas and A. C. Roger, Carbon dioxide methanation kinetic model on a commercial Ni/Al_2O_3 catalyst, *J CO_2 Util.*, 2019, **34**(March), 256–265, DOI: 10.1016/j.jcou.2019.05.030.

45 A. G. Bhavani, W. Y. Kim and J. S. Lee, Barium substituted lanthanum manganite perovskite for CO_2 reforming of methane, *ACS Catal.*, 2013, **3**(7), 1537–1544.

46 H. Gu, J. Ding, Q. Zhong, Y. Zeng and F. Song, Promotion of surface oxygen vacancies on the light olefins synthesis from catalytic CO_2 hydrogenation over Fe[sbnd]K/ZrO_2 catalysts, *Int. J. Hydrogen Energy*, 2019, **44**(23), 11808–11816, DOI: 10.1016/j.ijhydene.2019.03.046.

47 M. Matsuda, K. Katsumata, I. Watanabe and K. Nagamine, μSR measurements of $BaNiO_2$, *Hyperfine Interact.*, 1997, **104**(1–4), 97–103.

48 W. L. Vrijburg, G. Garbarino, W. Chen, A. Parastaev, A. Longo, E. A. Pidko, *et al.*, Ni-Mn catalysts on silica-modified alumina for CO_2 methanation, *J. Catal.*, 2020, **382**, 358–371, DOI: 10.1016/j.jcat.2019.12.026.

49 S. B. Ubale, T. T. Ghogare, V. C. Lokhande, T. Ji and C. D. Lokhande, Electrochemical behavior of hydrothermally synthesized porous groundnuts-like samarium oxide thin films, *SN Appl. Sci.*, 2020, **2**(4).

50 L. Dou, C. Yan, L. Zhong, D. Zhang, J. Zhang, X. Li, *et al.*, Enhancing CO_2 methanation over a metal foam structured catalyst by electric internal heating, *Chem. Commun.*, 2019, **56**(2), 205–208.